Accurate wavelengths for X-ray spectroscopy and the NIST hydrogen-like ion database

S. A. Kotochigova[*,†], K. P. Kirby[**,‡], N. S. Brickhouse[‡], P. J. Mohr[†] and I. I. Tupitsyn[§]

[*]*Department of Physics, Temple University, Philadelphia, PA 19122*
[†]*National Institute of Standards and Technology, 100 Bureau Drive, stop 8423, Gaithersburg, Maryland 20899*
[**]*Institute for Theoretical Atomic and Molecular Physics, 60 Garden St., Cambridge, MA 02138*
[‡]*Harvard-Smithsonian Center for Astrophysics, 60 Garden St., Cambridge, MA 02138*
[§]*St. Petersburg State University, Petrodvorets, 198504 Russia*

Abstract. We have developed an *ab initio* multi-configuration Dirac-Fock-Sturm method for the precise calculation of X-ray emission spectra, including energies, transition wavelengths and transition probabilities. The calculations are based on non-orthogonal basis sets, generated by solving the Dirac-Fock and Dirac-Fock-Sturm equations. Inclusion of Sturm functions into the basis set provides an efficient description of correlation effects in highly charged ions and fast convergence of the configuration interaction procedure.

A second part of our study is devoted to developing a theoretical procedure and creating an interactive database to generate energies and transition frequencies for hydrogen-like ions. This procedure is highly accurate and based on current knowledge of the relevant theory, which includes relativistic, quantum electrodynamic, recoil, and nuclear size effects.

Keywords: atomic data, X-ray emission spectra, Dirac-Fock theory, Sturmian functions, highly-charged ions of iron, hydrogen-like ions
PACS: 32.30.Rj

INTRODUCTION

This paper describes two different theoretical methods that we have developed to provide reliable and accurate atomic data needed for X-ray spectroscopy and astrophysical modeling. The first method is based on Multi-configuration Dirac-Fock-Sturm (MDFS) theory (see, for example, Refs. [1, 2] and references therein). It has unique features designed for efficient description of correlation effects in highly charged ions. The second method allows us to calculate highly accurate energies and transition frequencies of hydrogen-like ions, where correlation effects do not exist. Numerous relativistic and quantum electrodynamic (QED) corrections to the Dirac energy, together with nuclear size effects, have been included to obtain precise transition frequencies. This data will be available through a Physics Laboratory interactive web site at the National Institute of Standards and Technology.

We applied the MDFS method to calculate L-shell emission spectra of Fe XVIII up to Fe XXII. This work is part of the Emission Line Project at the Smithsonian Astrophysical Observatory to improve atomic databases for X-ray diagnostics. High quality observations from Chandra and XMM-Newton contain a wealth of emission lines which, if properly identified, can be used for determining plasma properties. The

L-shell emission spectra of iron have been relatively well studied by both theoretical and laboratory work (See for example Refs.[3, 4]). The accuracy obtained by these studies is very impressive. The best values of the transition wavelengths are determined with an accuracy of about 10^{-3} Å. At the same time the information provided is far from complete. For example, there are weak lines of Fe XIX between 13 Å and 14 Å, which have to be known better in order to understand their contribution to blends in the observed spectra. In addition, the resolution of laboratory measurements for Fe XX up to Fe XXII is not sufficiently high to avoid line blending in some spectral regions.

Our goal is to obtain information that can help to identify weak and blended lines in X-ray spectra of iron. The high accuracy that we expect to obtain is due to our computational approach, which is a combination of a relativistic MDFS and second order many-body perturbation theory (MBPT2) and includes an advanced treatment of correlation effects. In this presentation we focus on the calculation of energies and transition wavelengths only. The results for other properties such as oscillator strengths, photoionization and autoionization cross-sections are forthcoming.

MDFS THEORY

In our configuration interaction (CI) approach, the total wavefunction of an atom or ion is written as a linear combination of Slater determinants constructed from four component Dirac spinors and numerical Sturm functions:

$$\Psi(x_1, x_2, ..., x_N) = \sum_\alpha C_\alpha \det{}_\alpha \left(\phi(x_i)\right), \tag{1}$$

where N is the number of electrons and α counts the Slater determinants. The radial parts of the Dirac spinors or Sturm functions, $\phi(x)$, are obtained numerically by solving self-consistently either the Dirac-Fock or Dirac-Fock-Sturm equations. The coefficients C_α are obtained by solving a generalized eigenvalue problem by applying the iterative Davidson eigensolver. Higher-order correlation effects from highly excited orbitals, which are not included in the CI, are treated by second-order perturbation theory.

Dirac-Fock basis set

Dirac-Fock functions are chosen to describe the valence electrons and Sturm-Dirac functions represent the virtual orbitals. For example, Fe XIX has $1s^2\ 2s^2\ 2p^4$ electrons in the ground configuration and $1s^2\ 2s^2\ 2p^3$ 3s or 3p or 3d electrons in low-lying excited states of L-shell transitions. In our model all these valence orbitals are occupied. The valence orbitals are obtained by solving the Dirac-Fock (DF) equations. Higher-excited orbitals, such as 4s, 4p, 4d, and etc, if they are not occupied, play the role of virtual orbitals.

The use of DF functions as virtual orbitals has been shown to be ineffective. The radius of the excited DF orbitals grows rapidly with the level of excitation and becomes much larger than the radius of the valence orbitals. As a result the overlap between these orbitals is small, leading to slow convergence with an increase in the number of

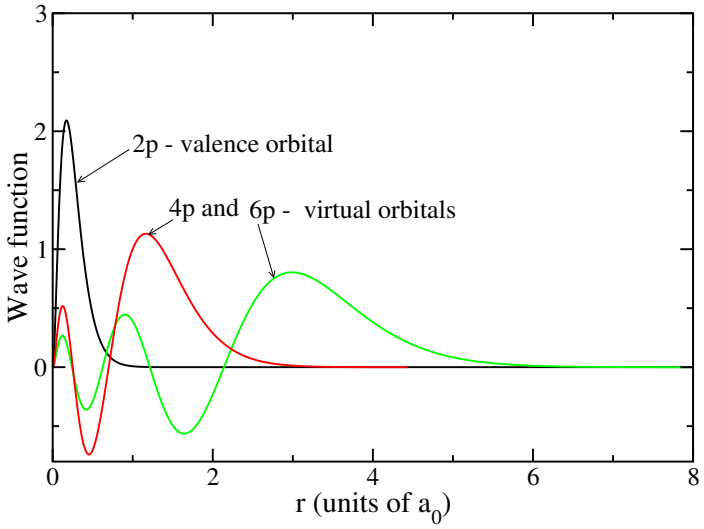

FIGURE 1. Dirac-Fock *p*-orbitals of Fe XIX.

orbitals in the CI procedure. Figure 1 shows the Dirac-Fock p orbitals of Fe XIX as an example. The 2p valence orbital is seen to have minimal overlap with the 4p and 6p virtual orbitals. The overlap between valence and virtual orbitals decreases as the principal quantum number n increases.

Sturm basis set

An alternative is to use Sturm functions obtained by solving the Dirac-Fock-Sturm equations, which are approximately given by

$$[H_{DF} - \varepsilon_0]\phi_j = \mu_j W_l(r)\phi_j \tag{2}$$

and solved for a fixed energy ε_0 equal to the energy of one of the valence electrons and fixed l. Here, H_{DF} is the Dirac-Fock part of the equation. The parameter μ plays the role of the eigenvalue of the Sturm operator. This operator is Hermitian and its eigenfunctions form a complete, discrete set of functions. We thus avoid the use of extended continuum functions. The l-dependent function $W_l(r)$ is a weight function with which the Sturm functions are orthogonalized:

$$\int_0^\infty dr W_l(r) P_{nl}(r) P_{n'l}(r) = 0\,, \quad n \neq n'. \tag{3}$$

In Refs [5, 6] W_l was chosen to have the form $1/r$, which works well for simple systems. However, this form has singularities at r=0 and slow convergence for $r \to \infty$. We have

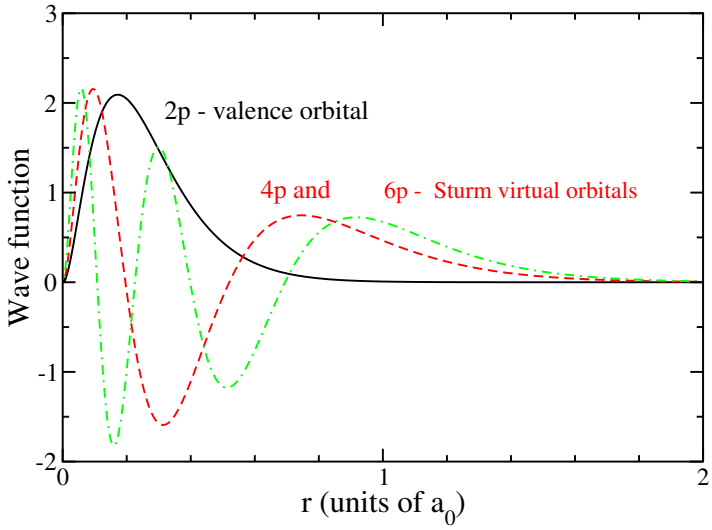

FIGURE 2. Dirac-Fock and Sturmian p-orbitals for Fe XIX.

found a better form for $W(r)$:

$$W_l(r) = -\frac{1-\exp(-[\alpha_l r]^2)}{[\alpha_l r]^2}\,. \tag{4}$$

This form approaches a constant for $r < 1/\alpha_l$ and decreases to zero more rapidly than $1/r$ as $r \to \infty$.

Figure 2 shows the Dirac-Fock 2p valence orbital and virtual 4p and 6p Sturm orbitals. Sturm functions are calculated using the ε_0 of the 2p valence orbital and are localized in the same spatial region as this reference function. They differ in the number of nodes. Near the core the functions are nearly identical and have a similar asymptotic behavior as the corresponding valence orbital. All these properties of Sturm functions help to construct efficient excited configurations that lead to a compact and rapidly convergent CI wave function.

COMPUTATIONAL MODEL

The Hamiltonian for the electrons contains three electron-electron operators. These are the Coulomb, magnetic, and retardation interactions. The basis sets are determined by including the Coulomb operator only. The magnetic and retardation contributions are then added for the CI calculation. Nuclear finite-size corrections are taken into account by using a Fermi charge distribution with parameters estimated from semi-empirical formulas using the Fe mass number.

We applied the MDFS+MBPT2 method to calculate wavelengths of L-shell transitions in Fe XVIII up to Fe XX. These spectra are sufficiently well understood from

combined experimental and theoretical studies. Once we are able to reproduce and even improve upon this data, we will be able to make predictions for spectral regions where the assignment is not certain.

The scale of the calculations is determined by the size of the Hamiltonian matrix. For all three cases of Fe XVIII, Fe XIX, and Fe XX we have used the same number of orbitals (46 relativistic orbitals) to construct the basis sets. However, the number of electrons in the 2p-shell differs and determines the size of the H-matrix. In the basis set not all orbitals are treated equally. Only orbitals from $1s^2$ up to 5d are used to construct configurations that appear in the CI. Higher excited orbitals, up to $n = 8$, are treated by second-order perturbation theory. For the Fe XIX $2p^3 3s$ calculation, for example, we have about 60 000 determinants in the Hamiltonian matrix and CI calculation. About 10^7 determinants are included using perturbation theory.

RESULTS AND COMPARISON

As a first step we have compared our calculations with results of an EBIT experiment and calculations with the HULLAC code, given in Ref. [3]. This is the most recent and complete study of the L-shell emission spectra of Fe XVIII to Fe XX. We show our results for the medium-sized calculation of Fe XIX 3s to 2p transitions. Figure 3 shows a number of lines with wavelengths ranging from 14.6 Å to 15.2 Å, which we are able to compare to the EBIT data and HULLAC calculations of Ref. [3]. The labels on the horizontal axis of Fig.3 correspond to a labeling of lines from the EBIT experiment. The markers connected by a full line show the wavelengths of our calculation. The markers connected by a dotted line correspond to HULLAC data and the error bars show the experimental results. Clearly, our calculations of transition wave lengths are consistently lower than HULLAC by a few hundredths of an Angstrom. We are in better agreement with experiment than HULLAC for most of the lines, with the exception of the $O9$ line. Table 1 lists the wavelengths as well as the quantum labels of $3s \rightarrow 2p$ transitions in Fe XIX obtained in our calculation and by Ref. [3].

Figure 4 shows a similar graph for the Fe XX spectrum. The line labels correspond to the notation of Ref. [3]. For the lines that have been assigned in the EBIT experiment the agreement between the three sources is similar to that for Fe XIX. The exception is the line between $N11$ and $N12$, which is very weak in the experimental spectrum. In addition, we note that our calculation shows many more $3s \rightarrow 2p$ transitions than are identified in Ref. [3]. To assign other observed lines with the help of our calculations we have to know the oscillator strength of each transition. This information will be forthcoming.

Figure 5 shows the Fe XVIII spectrum between 15.7 Å and 16.1 Å. Again we can see the same sort of agreement between the three sources. The two theoretical calculations differ significantly from experiment for the $F7$ line. This line, however, is reported as weak in the experimentally observed spectrum [3] and could have been assigned incorrectly.

The comparison of the MDFS calculations with data from Ref. [3] indicates that we reached 10^{-3} Å agreement with the experimental EBIT wavelengths for the three iron ions Fe XVIII, Fe XIX, and Fe XX. In our calculation we do not include QED

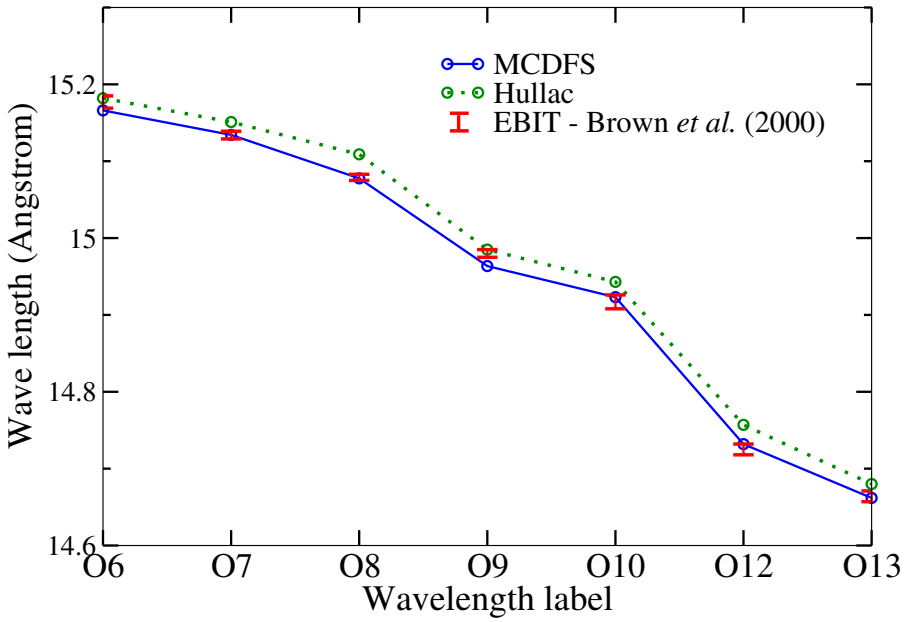

FIGURE 3. Wavelengths of $1s^2 2s^2 2p^3 3s \rightarrow 1s^2 2s^2 2p^4$ transitions in Fe XIX from our calculation and Ref. [3].

corrections. An estimate shows that these corrections are expected to be on the order of 10^{-3}-10^{-4} Å and therefore might be relevant. We plan to include the major QED corrections in our calculations in the near future. The systematic blue-shift of our wavelengths from HULLAC's data can be explained by the fact that the total energy of the ground states in our calculation is lower and according to the variational principal is more precise.

ENERGY LEVELS OF HYDROGEN-LIKE IONS

.

In this section, we describe the NIST project to create an interactive database, which provides theoretical values of energy levels and transition frequencies for hydrogen-like ions. The first phase of this project includes hydrogen-like ions from He^+ to Ne^{+9} and is planned to be completed in 2005. The values are based on the most recent knowledge of the relevant theoretical contributions to the Dirac energy of an electron, including relativistic, quantum electrodynamic, recoil, and nuclear size effects. Contributions that are known only for low principal quantum numbers n have been extrapolated to highly-excited states using techniques developed in our previous study of hydrogen and deuterium energy levels (see Refs. [7, 8]). The total list of contributions to the relativistic

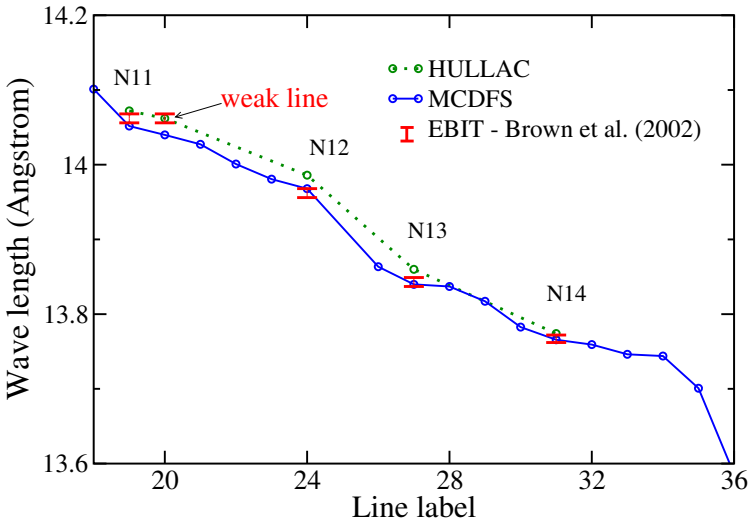

FIGURE 4. Wavelengths of $1s^2 2s^2 2p^2 3s \rightarrow 1s^2 2s^2 2p^3$ transitions in Fe XX. Our calculations are compared with results of Ref. [3]

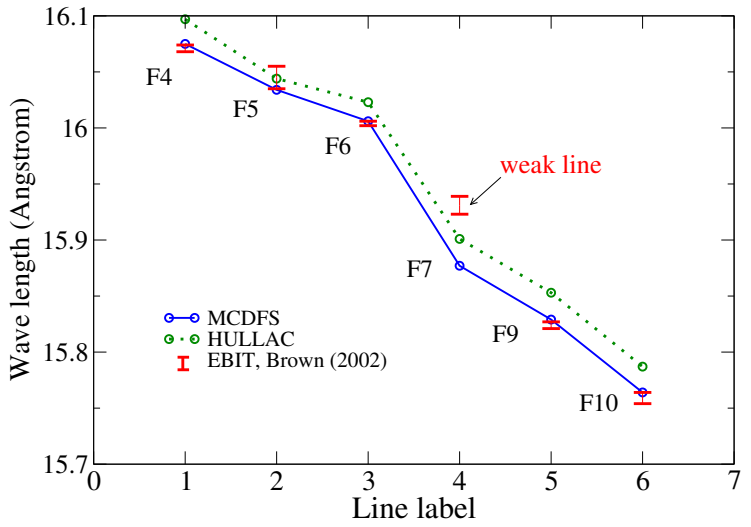

FIGURE 5. Wavelengths of $1s^2 2s^2 2p^4 3s \rightarrow 1s^2 2s^2 2p^5$ transitions in Fe XVIII. Our calculations are compared with results of Ref. [3]

TABLE 1. Wavelengths of $1s^2 2s^2 2p^3 3s \rightarrow 1s^2 2s^2 2p^4$ transitions in Fe XIX from our calculation and Ref. [3]. Columns 2 and 3 give the total angular momentum of the upper and lower state of the transition.

Line label	Upper J	Lower J	MDFS	HULLAC	EBIT
	2	1	15.283		
*O*6	1	1	15.167	15.182	15.177(8)
*O*7	1	0	15.134	15.151	15.134(5)
*O*8	2	2	15.078	15.109	15.079(4)
*O*9	1	2	14.964	14.985	14.980(5)
	2	1	14.928	14.948	
	1	1	14.923	14.943	14.917(9)
	1	0	14.892		
	2	1	14.813		
*O*12	2	2	14.732	14.757	14.725(7)
	1	2	14.727		
	0	1	14.668		
*O*13	3	2	14.662	14.680	14.664(7)

TABLE 2. List of relativistic and QED contributions used in calculations of hydrogen-like ion energy levels

Relativistic Recoil	Self Energy
Vacuum Polarization	Two-photon Corrections
Three-photon Corrections	Finite Nuclear Size
Radiative-Recoil Correction	Nuclear Size Correction
Nuclear Polarization	to Self Energy and
Nuclear Self Energy	Vacuum Polarization

Dirac energy is given in Table 2. Detailed descriptions of these contributions will be given in a forthcoming publication. The present study is limited to levels with principal quantum numbers $n = 1$ to 20 and all allowed orbital angular momenta ℓ and total angular momenta j.

Fundamental constants used in the theoretical expressions are taken from the 2002 least squares adjustment published on the Fundamental Physical Constants NIST web site. The nuclear parameters needed for the evaluation of the hydrogenic energy levels are the mass and charge radius. To obtain the nuclear mass, we take the atomic mass from the 2003 update of the atomic mass evaluation of Refs. [15, 16]. The atomic mass data are also available in an electronic version at www−csnsm.in2p3.fr/amdc/web/masseval.html, the Web site of the Atomic Mass Data Center (AMDC) Centre de Spectrométrie Nucléaire et de Spectrométrie de Masse (CSNSM), Orsay, France. The values of the atomic masses are given in the first column of Table 3.

A calculation of the relative masses of various nuclei requires the total ionization energies, or binding energies $E_{\rm b}$ (the sum of the individual ionization energies). These are calculated by summing the ionization energies of each stage of ionization of a given atom, and the results are given in the second column of Table 3.

TABLE 3. Atomic and nuclear parameters obtained from the literature

Z	Atomic mass (a.m.u.)	Ionization energy (cm^{-1})	Nuclear radius (fm)
1	1.007 825 032 07(10)	109 678.7717	0.852 1(70)
2	4.002 603 254 15(6)	637 219.638 4	1.675 8(27)
3	7.016 004 548(84)	1 641 227.159 2	2.395 2(510)
4	9.012 182 201(426)	3 219 335.722 4	2.518 0(116)
5	11.009 930 540 6(448)	5 411 855.820 6	2.405 9(293)
6	12	8 308 360.968 9	2.470 4(23)
7	14.003 074 004 78(62)	11 985 917.103 2	2.552 0(85)
8	15.994 914 619 56(16)	16 484 719.293 5	2.702 8(76)
9	18.998 403 224(74)	21 904 891.239 8	2.897 6(27)
10	19.992 440 175 42(192)	28 323 307.502 2	3.004 6(38)

The nuclear root-mean-square (rms) charge radii are given in the last column of Table 3. They are taken from the compilation of Angeli [17].

Uncertainties in the energies and transition frequencies are estimated. They take into account uncertainties in the theoretical calculations and in the fundamental constants.

As an example of the available data on hydrogen-like ions Fig. 6 shows a comparison of our theoretical values for the Lamb shift and experimental data. References to the experimental data are given in the caption of Fig. 6.

ACKNOWLEDGMENTS

We acknowledge helpful discussions with Tim Kallman and Patrick Palmeri.

REFERENCES

1. S. A. Kotochigova and I. I. Tupitsyn, *J. Phys. B: At. Mol. Phys.*, **20**, 4759-4772 (1987).
2. S. Kotochigova, E. Tiesinga, and I. Tupitsyn, in "New Trends in Quantum Systems in Chemistry and Physics" **1** (Kluwer Academic Publ., The Netherlands), (2001), pp. 219-242.
3. G. V. Brown, P. Beiersdorfer, D. A. Liedahl, K. Widmann, S. M. Kahn, and E. J. Clothiaux, *ApJ Supp. Ser.*, **140**, 589-607 (2002).
4. T. Shirai, Y. Funatake, K. Mori, J. Sugar, W. L. Wiese, and Y. Nakai, *J. Phys. Chem. Ref. Data*, **19**, 127-257 (1990).
5. V. A. Fock, in *Principles of Quantum Mechanics*, (1976)
6. R. Szmykowski, *J.Phys.B*, **30**, 825-861 (1997)
7. S. Kotochigova, P. J. Mohr, and B. N. Taylor, *Can. J. Phys.*, **80**, 1373-1382 (2002).
8. S. Kotochigova, P. J. Mohr, and B. N. Taylor, at http://physics.nist.gov/PhysRefData/HDEL (2004)
9. S. R. Lundeen and F. M. Pipkin, *Metrologia*, **22**, 9-54 (1986).
10. A. van Wijngaarden, F. Holuj, and G. W. F. Drake, *Phys. Rev. A* **63** 012505 (2001)
11. M. Leventhal, *Phys. Rev. A*, **11**, 427-441 (1975).
12. H. W. Kugel, M. Leventhal, and D. E. Murnich, *Phys. Rev. A*, **6**, 1306-1321 (1972).
13. B. Curnutte, C. L. Cocke, and R. D. Dubois, in "Proceedings of Int. Conf. Fast Ion Beam Spectr.", Laval (1981).
14. H. W. Kugel, M. Leventhal, D. E. Murnich, C. K. N. Patel, and O. R. Wood, *Phys. Rev. Lett.*, **35**, 647-650 (1975).

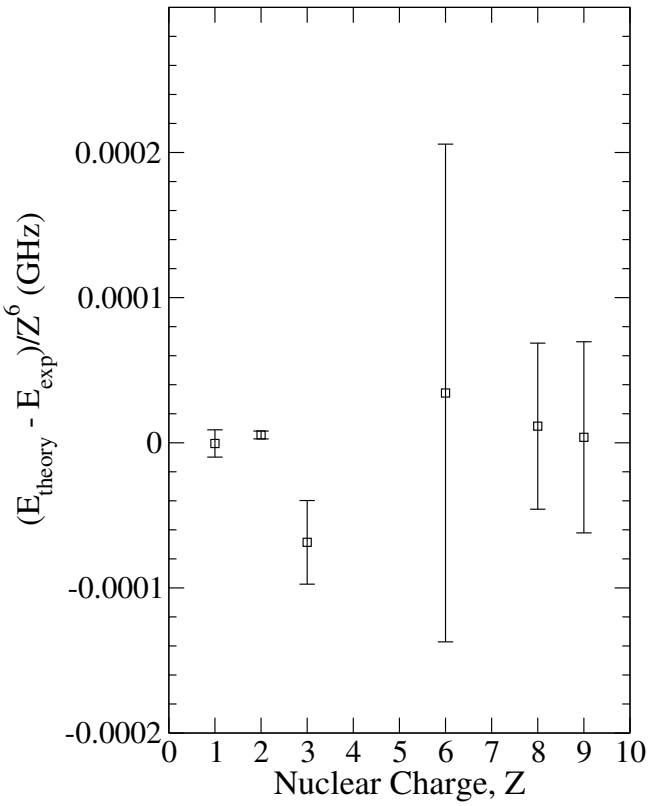

FIGURE 6. The Lamb shift difference between our theoretical values and experimental data for hydrogen and hydrogen-like ions. The experimental data are taken from Refs.: H - [9], He^{+} - [10], Li^{+2} - [11], C^{+5} - [12], O^{+7} - [13], and F^{+8} - [14]. The error bars primarily show experimental uncertainties.

15. A. H. Wapstra, G. Audi, and C. Thibault, *Nucl. Phys. A*, **729**, 129-336 (2003).
16. G. Audi, A. H. Wapstra, and C. Thibault, *Nucl. Phys. A*, **729**, 337-676 (2003).
17. I. Angeli, *Heavy Ion Physics*, **8**, 23-29 (1998).